Magnetic Microstructure of Rolled-Up Single-Layer Ferromagnetic Nanomembranes

Robert Streubel, Jehyun Lee, Denys Makarov, Mi-Young Im, Daniil Karnaushenko, Luyang Han, Rudolf Schäfer, Peter Fischer, Sang-Koog Kim, and Oliver G. Schmidt*

Inorganic nanomembranes are stretchable,[1] shapeable,[2] and transferrable to virtually any substrate.[3,4] These properties build the core concept for new technologies that transform otherwise rigid high-speed devices into their flexible counterparts. Whereas semiconductor nanomembranes have been implemented in a wealth of different applications,[1,5] magnetic nanomembrane devices are much more scarce. We recently demonstrated flexible and stretchable magnetoelectronic devices based on thin-multilayer giant magnetoresistive (GMR) and spin-valve nanomembranes.[6–10] By proper strain engineering, magnetic nanomembranes can also be rolled up into microtubes.[11–14] In this way, compact three-dimensional GMR sensors[15,16] for magnetofluidic applications,[15] spin-wave filters,[13,17] and remotely controlled microrobots[18] have been realized.

Apart from their potential for applications, carefully designed rolled-up magnetic nanomembranes are of great fundamental interest, since they can be magnetized into unique radial and chiral configurations.[19] A thorough understanding of the micromagnetic properties of rolled-up magnetic nanomembranes is lacking, as their magnetic state is usually derived from macroscopic hysteresis curves.[20,21] It was recently demonstrated theoretically[22] that the speed of domain walls, for example, in a magnetic racetrack memory,[23] can be significantly increased when using magnetic wires of cylindrical cross-section with a diameter of less than 50 nm. Theoretical studies on closed-tubular and rodlike structures of sub-100-nm-range diameter reveal that the number of domain states is considerably reduced from that in larger structures, which substantially simplifies theoretical considerations.[22,24,25] Investigations of larger tubes have not been undertaken, due mainly to limitations in computing power and the lack of consistent experimental data. The magnetic microstructure of a rolled-up tube is expected to be more complex than that of a closed one. Recently, first experimental studies were carried out to identify magnetic states in individual tubular structures of 150 nm diameter prepared by anodization. Even for these rather small tubular architectures, the authors had to consider six distinct magnetic states in explaining their experimental findings.[26,27] The present study considers larger diameters of tubular architectures, which result in an increase both of the number of possible magnetic states and of their complexity.

Here and for the first time, we reveal both theoretically and experimentally the magnetic microstructure of rolled-up magnetic nanomembranes of micrometer-range diameter. According to the initially deposited layer (single magnetic layer or heterostructured magnetic–non-magnetic bilayer), two fundamentally different rolled-up microtube geometries can be achieved. In the case of the single magnetic layer a closed tube is obtained, where the magnetic response between the overlapping layers is governed by short-range exchange coupling as well as long-range magnetostatic interactions. In contrast, when an exchange-breaking non-magnetic spacer layer is added, the magnetic phenomena are determined only by the magnetostatic interaction between adjacent windings of the rolled-up nanomembrane that depends on the interface roughness (so-called orange-peel coupling).[28] By tuning the thickness of the non-magnetic spacer layer, the magnetic interactions between cylindrically arranged layers can be gradually modified. In the case of conducting spacer layers, indirect Ruderman–Kittel–Kasuya–Yosida (RKKY) coupling[29,30] might play an important role in addition to dipolar coupling.

The rolling-up technology relies on thin-film deposition techniques like sputtering to achieve magnetic tubes with high structural quality and low surface roughness. This dependence enables us to investigate magnetic properties that are emergent in tubular architectures, where the domain pattern is not affected by the structural inhomogeneity due to the granular nature of the magnetic thin film that leads to pinning of magnetic domains, as known for anodization-based

R. Streubel, Dr. D. Makarov, D. Karnaushenko, Dr. L. Han, Prof. O. G. Schmidt
Institute for Integrative Nanosciences
IFW Dresden, 01069, Dresden, Germany
E-mail: d.makarov@ifw-dresden.de
R. Streubel, Prof. O. G. Schmidt
Material Systems for Nanoelectronics
Chemnitz University of Technology
09107, Chemnitz, Germany
Dr. J. Lee, Prof. S.-K. Kim
National Creative Research Initiative Center for Spin Dynamics and Spin-Wave Devices
Nanospinics Laboratory
Research Institute of Advanced Materials
Department of Materials Science and Engineering
Seoul National University
Seoul, 151–744, South Korea
Prof. R. Schäfer
Institute for Metallic Materials
IFW Dresden, 01069, Dresden, Germany
Prof. R. Schäfer
Institute for Materials Science
TU Dresden, 01069, Dresden, Germany
Dr. M.-Y. Im, Dr. P. Fischer
Center for X-ray Optics
Lawrence Berkeley National Laboratory
Berkeley, California, 94720, USA

DOI: 10.1002/adma.201303003

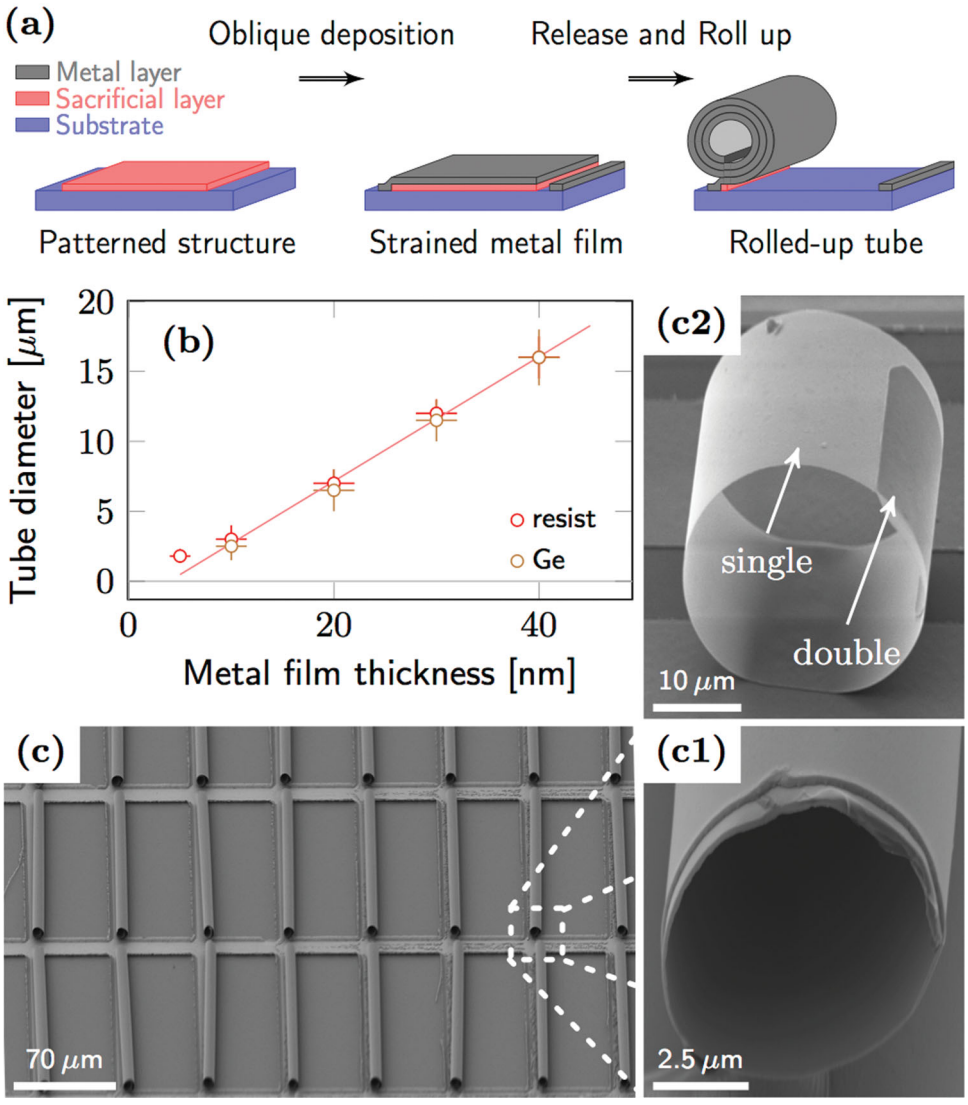

Figure 1. Fabrication of rolled-up single-layer ferromagnetic nanomembranes: a) The ferromagnetic film is deposited at an oblique angle onto a sacrificial layer. The internal strain is adjusted to roll-up the single-layer nanomembrane after selective release. b) The diameter of the rolled-up nanomembrane is determined by the film thickness. c) Optimized fabrication conditions result in a rolled-up tube yield of more than 90% and negligible spacing between windings [see also magnified view in (c1)]. c2) A rolled-up Py tube with an approximately 1.2 windings, revealing that the adjacent windings are in firm mechanical contact over the entire length of the tube.

architectures.[31] Herein, we focus on the investigation of magnetic states in closed tubes prepared by using rolled-up technology.

Firstly, we fabricated rolled-up ferromagnetic nanomembranes that consisted of a single ferromagnetic layer without an auxiliary spacer layer between the ferromagnetic windings to achieve an entirely ferromagnetic architecture. Using Ni and Py evaporation materials, we tailored both the sign and magnitude of magnetostriction within the nanomembrane, and thus the strain-induced anisotropy. The final geometry of the nanomembranes was predefined by patterning the underlying sacrificial layer, of positive photoresist (ARP 3510) or Ge, which created an initial planar, rectangular nanomembrane (**Figure 1**a). Subsequently, the planar magnetic nanomembranes rolled-up and formed into compact tubes without a gap between the windings (Figure 1c1 and 1c2). The oblique incidence of the evaporated magnetic material at an angle of 60° with respect to the surface normal, along with an increasing deposition rate (0.4–1.5 Å s^{-1}), induces a compressive strain within the magnetic film parallel to the incidence plane. The strain is largest at the bottom surface of the film and smallest at the top. This gradient is crucial to initiation of the rolling process in *N*-methyl-2-pyrrolidone (NMP) when using photoresist, or in 3% H_2O_2 when using the Ge sacrificial layer. To prevent collapse of the tubes during drying, the solvent was replaced by CO_2 that had been dried at its critical point. Tube diameters in the 2–16 μm range were obtained by varying the film thickness of Ni and Py from 5 to 40 nm. For a film thickness larger than 10 nm, a linear relation between thickness and tube diameter was observed (Figure 1b). The deviation from the linear trend for very thin layers is due to the saturation of the strain within the polycrystalline film. The error bars reflect the distribution of the tube diameters.

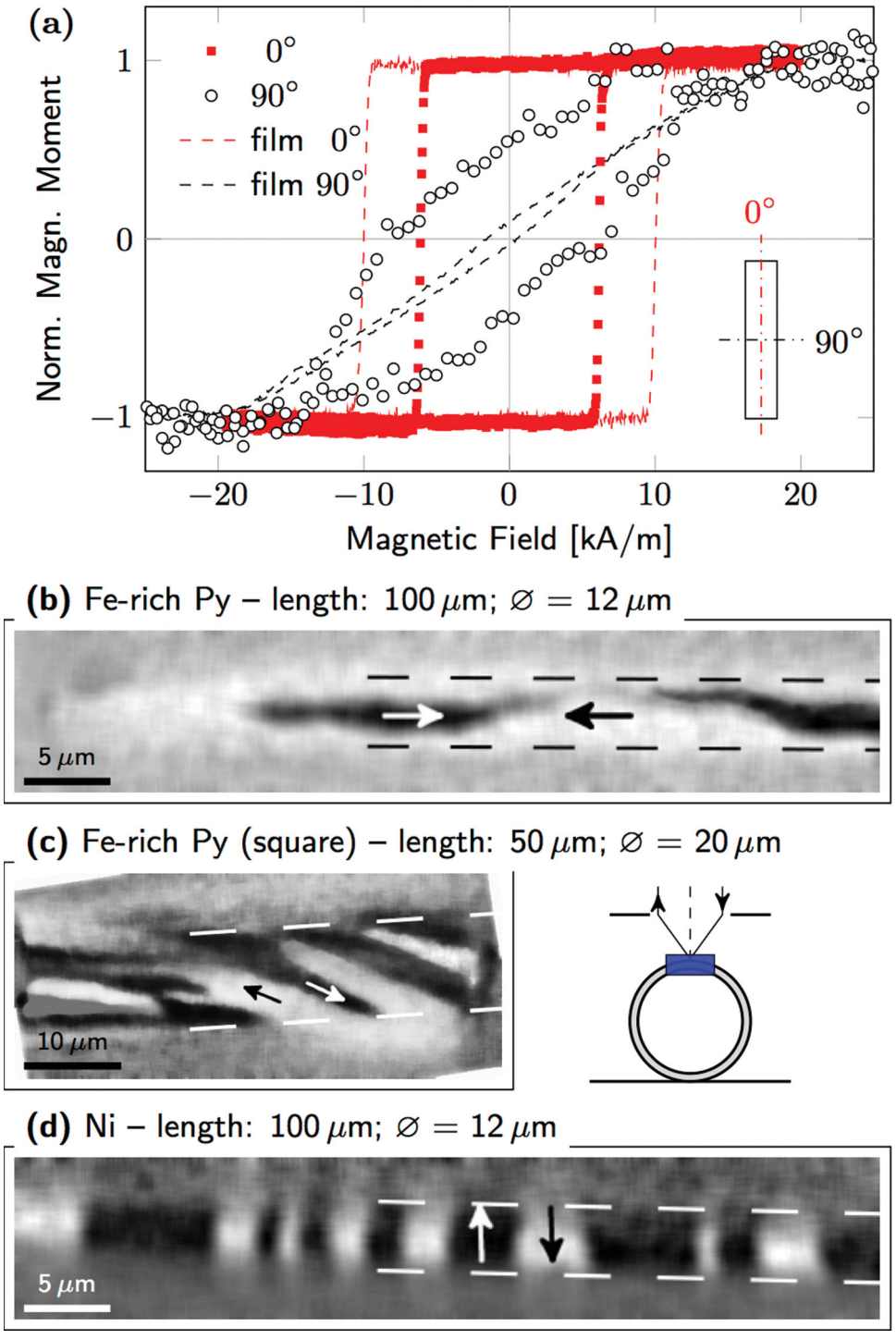

Figure 2. Magneto-optical characterization of rolled-up tubes: a) Magnetic hysteresis loops measured using longitudinal MOKE magnetometry of extended Fe-rich Py films (dashed lines) and rolled-up nanomembranes (symbols). The magnetic-domain patterns were visualized by Kerr microscopy and imaged at remanence after ac demagnetization of the samples: b) Fe-rich Py with magnetization along the tube axis and c) spiral-like magnetic domains with oblique magnetic-domain walls in a shorter rolled-up Fe-rich Py nanomembrane. The inset in (c) illustrates the limitation of visualization (blue area in focus) when using Kerr microscopy on tubular architectures. d) Ni tubes with azimuthally aligned 180° magnetic domains.

Optimized preparation conditions result in an array of rolled-up nanomembranes with a yield of more than 90% and negligible spacing between the windings (Figure 1c2).

The magnetic properties were investigated by means of longitudinal magneto-optical Kerr effect (MOKE) magnetometry. **Figure 2**a shows the magnetic hysteresis loops of a 20 nm-thick Py nanomembrane rolled up into a 100 μm-long tube of 7 μm diameter and consisting of 2.5 windings. Hysteresis loops taken of a reference sample before rolling are also given. The spot size of the focused beam in the MOKE set-up was

approximately 10 μm, which allows us to study the magnetic response of individual rolled-up architectures. This method brings obvious advantages compared to the commonly applied integral magnetic characterization methods (e.g., vibrating sample magnetometry (VSM)), where the signal provides only information averaged over a large array of tubes. The MOKE measurements were performed by applying an external magnetic field parallel (0°) and perpendicular (90°, in-plane) to the tube axis. The coercive fields of the evaporated Py samples of about (10.0 ± 0.2) kA m^{-1} (Figure 2a) are substantially larger than those typically obtained for magnetron-sputter-deposited Py films.[32] Due to the larger evaporation pressure of nickel (Ni) than iron (Fe) , e-beam vapor deposition of a permalloy target (original composition: $Ni_{80}Fe_{20}$) results in an NiFe alloy with an Fe concentration exceeding the original one (hereafter, Fe-rich Py film).[33] These magnetic films exhibit a positive magnetostriction constant[34] that imparts strain-induced uniaxial anisotropy to the system. An analysis of the hysteresis loops of the planar nanomembrane (dashed lines) reveals a magnetic easy axis in the rolling direction (0°). The strain-induced anisotropy constant can be estimated from the area under the hard-axis and easy-axis hysteresis loops, resulting in K_P = (10.1 ± 0.5) kJ m^{-3} and K_T = (7.5 ± 0.5) kJ m^{-3} for the planar and rolled-up nanomembranes, respectively. By using these values, we have estimated the compressive strains in the deposition direction as ε_P = (9 ± 3) ‰ and ε_T = (7 ± 2) ‰. To calculate the strain, the equation for the magnetostrictive anisotropy $K = 3/2\lambda\varepsilon Y$ is applied, with the magnetostriction constant $\lambda = 5 \times 10^{-6}$ and the Young's modulus Y = 100 GPa for electroplated Py.[34,35] Interestingly, the coercive field of the rolled-up nanomembrane measured in the easy-axis direction, $H_{C,T}$ = (6.1 ± 0.2) kA m^{-1}, was found to be smaller than that of the reference planar film, $H_{C,P}$ = (10.0 ± 0.2) kA m^{-1}. We attribute this observation to the fact that the transformation from planar into rolled-up architecture is accompanied by the lowering of the strain-induced anisotropy as discussed above.

The peculiar magnetization configurations of the rolled-up nanomembranes were visualized by Kerr microscopy. Due to the limited probing depth of this imaging technique,[36] only information about the magnetic state of the outer layer of the three-dimensional rolled-up architecture can be obtained. Kerr microscopy is widely used to investigate the ground state, switching behavior, and magnetization dynamics in planar magnetic films. Here, we show that this method is also suitable for the observation of magnetization configurations on curved magnetic surfaces of rolled-up architectures with a diameter down to 10 μm. Due to the curvature, only a narrow stripe on top of the tube can be focused during imaging [Figure 2, inset in (c)]. The magnetic-domain patterns in Fe-rich Py and Ni rolled-up nanomembranes (length: 100 μm; diameter Ø: 12 μm), obtained at remanence after ac demagnetization, are shown in Figure 2b and 2d, respectively. The magnetization orientation within the dark and bright domains is indicated by arrows. For a rolled-up nanomembrane of 100 μm length, a magnetic domain pattern with magnetization in domains oriented along the tube axis is observed (longitudinally magnetized domains). By changing the dimensions of the planar nanomembrane, we tailor the length of the rolled-up architecture, thereby altering the magnetic shape anisotropy of the sample. A Kerr microscopy image of the rolled-up Fe-rich Py tube of 50 μm length and 20 μm diameter is shown in Figure 2c. The magnetic contrast reveals a domain pattern with obliquely aligned domain walls, which can be attributed to the spiral-like magnetic domains. Furthermore, the experimental study shows that, while the magnetic moment of rolled-up Fe-rich Py is aligned preferentially along the tube axis, the Ni sample manifests azimuthally aligned 180° domains (Figure 2d). The domain type (longitudinal, azimuthal, or spiral-like) was found to be independent of the tube diameter in the investigated range from 2–16 μm (not shown). This observation can be understood as follows: the orientation of the magnetic moment in the domains is along the easy axis, which is defined by the interplay between the stress-induced and shape anisotropies. The shape anisotropy in hollow tubular structures is determined mainly by the thickness of the magnetic membrane and the length of the tube. Our results indicate that the most efficient way to tune the type of domains is to change the length of the rolled-up tube as shown in Figure 2.

The experimentally observed domain structures for the rolled-up Py and Ni nanomembrane are well reproduced by micromagnetic simulations. We simulated the magnetic microstructure of rolled-up tubes using the FEMME software.[37] The remanent magnetic states are obtained by zero-field relaxation from two initial magnetization patterns: 1) a random distribution of magnetic moments, and 2) a predefined two-domain magnetic state. The planar 20-nm-thick nanomembranes are rolled up into tubular architectures of 600 nm diameter and 2500 nm length. The dimensions of the simulated structures are smaller than the experimental ones due to computational limitations. However, the chosen dimensions are sufficiently large to qualitatively capture the governing physics. In fact, dimensions of already hundreds of nanometers are sufficiently large to contain the typical local spin patterns of magnetic domain walls, as well as vortex and antivortex spin configurations.[38–41] The material parameters of permalloy (Py, $Ni_{80}Fe_{20}$ alloy) are assigned to the models: saturation magnetization 860 kA m^{-1}, exchange coefficient 13 pJ m^{-1}.[42] Based on the experimental data, a small uniaxial anisotropy along the tube axis of 6 kJ m^{-3} is taken into account. Since the value used for the magnetic anisotropy constant was adopted from the experiment, it includes also magnetostrictive contributions.

In the case of tubes without spacer (as in the experiment), Landau-closure-domain structures are formed after relaxation from both initial configurations (**Figure 3**a,b). There is, however, a significant difference in the structure and orientation of the basic domain walls: obliquely running, low-angle Néel walls are found after relaxation from random initial magnetization (Figure 3a), whereas relaxation from a two-domain state results in 180° domains that are separated by cross-tie-type domain walls (Figure 3b). Both wall types are attributed to the specific wall energy of Néel walls, which are expected in our films with a thickness of 20 nm. Geometrically, domain patterns with 180° Néel walls that run along the tube axis would lead to the lowest wall length, but a 180° Néel wall can significantly save energy by forming cross-ties. A cross-tie wall consists of alternating segments of low-angle Néel walls (the specific wall energy of a 90° Néel wall is only 12 % of that of an 180° wall[36] that is separated by vortex and antivortex spin configurations, which

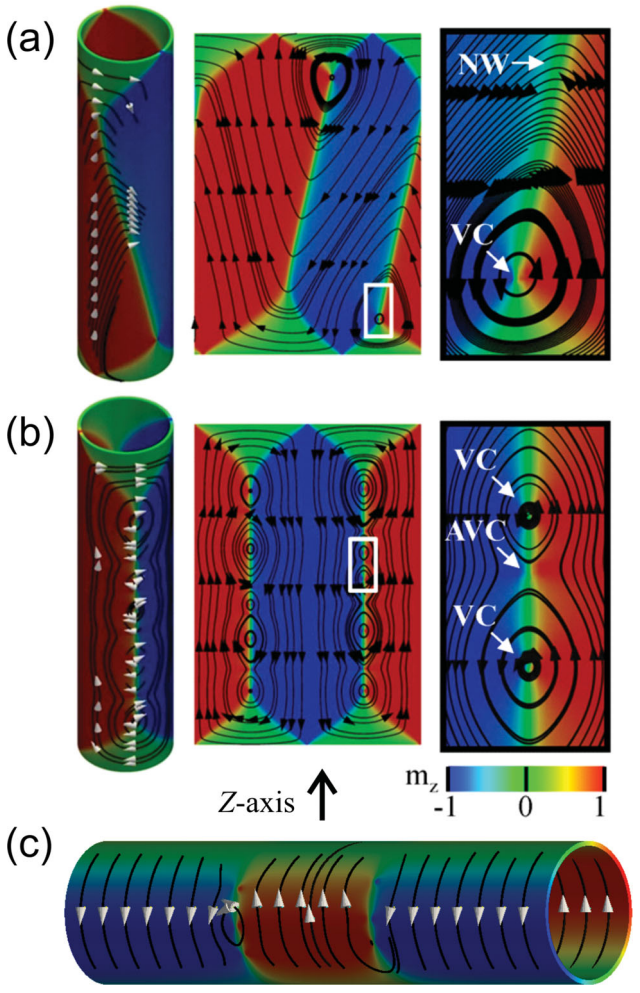

Figure 3. The magnetic domain patterns of rolled-up permalloy and Ni nanomembranes for the model without a spacer. The domain configurations for the permalloy tube were obtained from two initial magnetization patterns: a) random distribution of magnetic moments and b) a predefined two-domain magnetic state, wherein half of the spins point in the +*z* and the other half in the –*z* direction. The local spin orientations inside of the white boxes are magnified on the right side, with indications of Néel wall (NW), vortex core (VC), and antivortex core (AVC). c) Remanent domain pattern of the Ni tube after relaxation from the random initial state.

contribute to the total wall energy. In the magnetic pattern shown in Figure 3a, a low-angle, homogeneously magnetized Néel wall is formed that runs oblique to the tube axis. From our micromagnetic calculations, the total energy of the oblique domain structure is slightly lower than that with the cross-tie walls (ΔE_{total} = (–2.105) – (–1.927) = –0.178 kJ m^{-3}). The negative sign of the energy originates from the definition of anisotropy energy E_{ani} in FEMME, where the maximum anisotropy energy is zero; therefore, E_{ani} is negative when some magnetization vectors in the model align along the easy axis. Both cross-tie and oblique low-angle walls are only favorable for very low magnetic anisotropy, which applies to our tubes. There is a significant difference with respect to flat patterned elements: a magnetization configuration as in Figure 3a would not be possible in a regular low-anisotropy rectangular element with some longitudinal anisotropy. In such a case, the magnetization is parallel to the element edges to avoid edge poles, thus enforcing a 180°-wall basic domain pattern. The additional degree of freedom of oblique low-angle domain walls is only possible for tubular geometry.

Considering the energy contributions, the oblique domains would be less preferable when the anisotropy along the tube is increased, for example in the case of field- or strain-induced anisotropy or shape anisotropy (longer tube). These simulation data correctly capture experimental findings on Fe-rich Py tubes (Figure 2b,c). Indeed, the magnetization is aligned along the tube axis when the tube is long (the combined effect of the shape- and stress-induced anisotropies), and, when the shape anisotropy decreases, there is a clear state with oblique magnetic-domain walls. The magnetic state characteristic of the rolled-up Ni nanomembrane can be captured by simulation as well (Figure 3c). The cause of the azimuthally aligned 180° domains is the negative magnetostriction coefficient, which results in a 90° rotation of the easy axis with respect to Fe-rich Py films.

To obtain information on the magnetization reversal behavior of the entire rolled-up nanomembrane, electrical transport measurements were conducted on individual rolled-up Fe-rich Py and Ni single-layer architectures. The tubes were transferred onto electric contacts with the aid of a micromanipulator in a cross-beam workstation, and were contacted using focused-ion-beam (FIB)-activated Pt deposition (**Figure 4**a). Measurements were performed by application of a 10 mA *dc* current to the sample, which corresponds to a current density of about 10^6 A cm^{-2}. Magnetoresistance (MR) curves drawn of the Fe-rich Py sample for two different perpendicular alignments with respect to the applied magnetic field (90°; in out-of-plane direction: oop) match very precisely (Figure 4b). This finding, combined with the characteristic shape of the MR curve measured with a longitudinally applied magnetic field (0°), suggests that the system possesses a uniaxial magnetic anisotropy with an easy tube axis, similar to the observation by Rüffer et al.[26] The two minima on the MR curve obtained in the longitudinal magnetic field (0°) correspond to the coercive field values of the MOKE magnetic hysteresis loop (Figure 2a). The magnetoresistive response of the rolled-up single-layer Ni nanomembrane of the same dimensions is substantially different from that in the case of Fe-rich Py (compare Figure 4b,c). Additional to the strongly modified response along the tube axis (0°), the measured curves perpendicular to the tube exhibit hysteresis, as expected for azimuthally magnetized architectures, which thus confirms the conclusion drawn from the MOKE measurements.

The versatility of the proposed fabrication technology allows the preparation not only of closed tubes, but also tubes with a spacer. We realized tubular structures out of a single 10-nm-thick Ni nanomembrane, which is rolled into a tube with a spacer between the windings (not tightly rolled tubes). To achieve this type of rolling process, the deposition procedure was slightly modified by using Ni alloyed with a small amount of carbon. The addition of C reduces the strain in the metal film, which in turn increases the diameter of the tubular architectures. As a result, the saturation magnetization is reduced but the size of the magnetic domains also decreases below the resolution limit of magneto-optical microscopy. To gain detailed

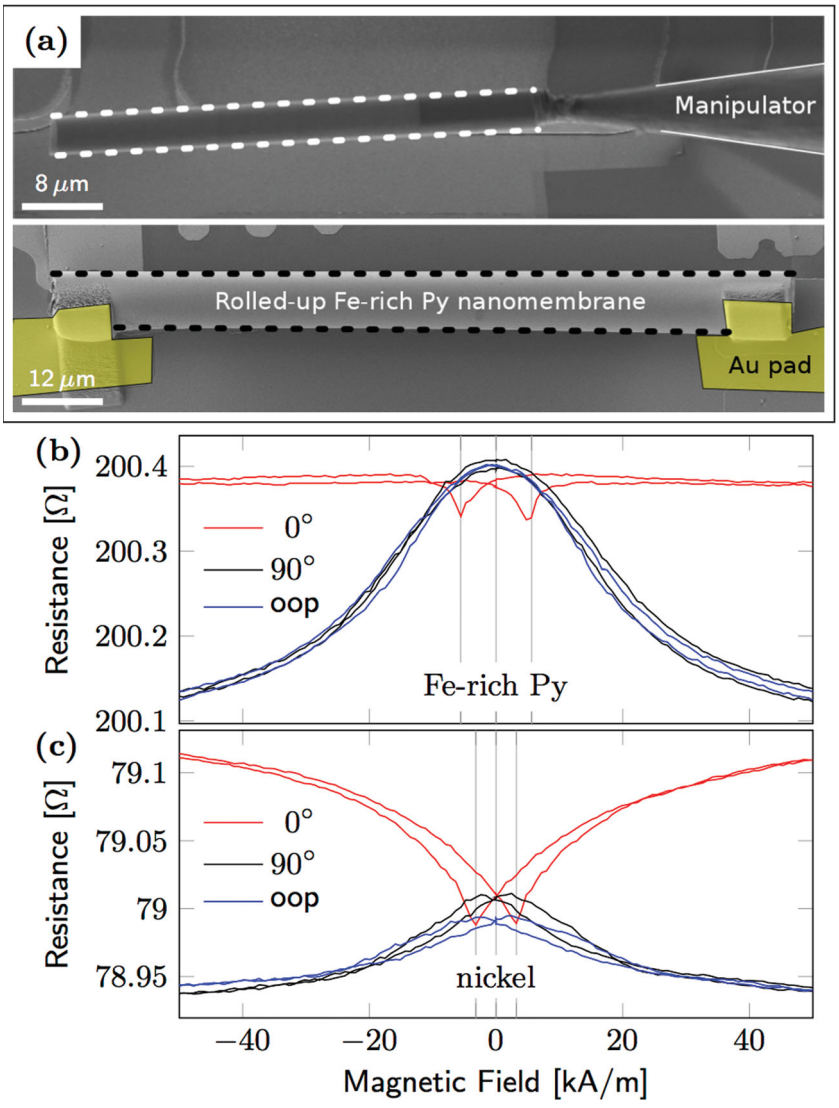

Figure 4. Electrical-transport measurements through individual rolled-up architectures: a) Transfer of a rolled-up nanomembrane with the aid of a micromanipulator (top panel) and the measured contacted tube (bottom panel), magnetoresistance curves of rolled-up 20-nm-thick b) Fe-rich Py, and c) Ni single-layer nanomembranes.

insight into the magnetic switching behavior of those samples, high-resolution magnetic full-field soft X-ray transmission microscopy (M-TXM), was performed using beamline 6.1.2. (XM-1) at the Advanced Light Source in Berkeley, CA, USA. This imaging technique combines elemental and magnetic sensitivity due to X-ray magnetic circular dichroism, which is used as a strong magnetic contrast mechanism with high spatial and time resolution,[43,44] where state-of-the-art Fresnel zone plates as optical elements have demonstrated a spatial resolution down to 15 nm[45] for magnetic imaging. Here we report the first attempt to use M-TXM for magnetic tomography, by applying a through-focus scanning mode by taking advantage of the depth of focus of the zone plate objective lenses used here below 1 μm and a penetration length of several 100 nm for X-rays with energies of about 1 keV. These values correspond to resonant X-ray absorption *L*-edges for typical magnetic materials, such as the 3d transition metals Fe, Co, Ni. As this is a photon-only technique, magnetic fields can be applied during recording, which allows saturation of the magnetization in the specimens. The micrographs shown in **Figure 5** are the first reported M-TXM images of three-dimensional magnetic structures, indicating the potential of this new approach. Two series of samples were characterized: 1) with the tube axis along the anisotropy axis and 2) with the tube axis perpendicular to the anisotropy axis. With the magnetic easy axis perpendicular to the tube axis, small azimuthally aligned 180° magnetic domains can be clearly observed in Ni tubes (Figure 5a). This finding is similar to the observation in Figure 2d. In contrast, when the easy axis is aligned along the tube axis, longitudinal domains are measured (Figure 5b). This case is similar to the case of Fe-rich Permalloy tubes (Figure 2b).

We have investigated both theoretically and experimentally specific magnetic domain patterns emerging in rolled-up magnetic nanomembranes with and without non-magnetic spacer layers. The magnetic response of the rolled-up architecture with a non-magnetic spacer is governed by magnetostatic interactions. In contrast, the magnetic behavior of closed tubes without a spacer layer is driven by exchange interactions. Interestingly, a clear degeneracy of magnetic ground states was found theoretically in the case of closed-tube structures. We fabricated rolled-up single-layer ferromagnetic nanomembranes of micrometer-range diameters. By using materials with different magnetostriction constants (i.e., Ni and Fe-rich Py) and varying the shape

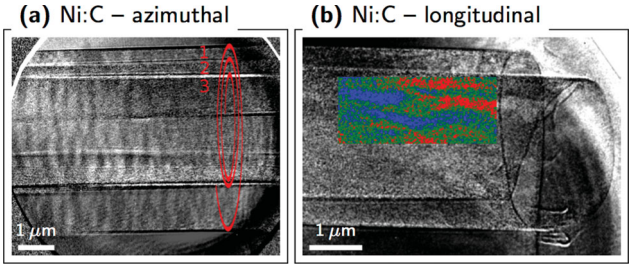

Figure 5. M-TXM images of a 20 nm-thick rolled-up Ni film alloyed with carbon. Magnetic easy axis is a) perpendicular and b) parallel to the tube axis. Imaging is carried out at remanence. Red line in (a) schematically shows the winding of the tube. Orientation of the magnetic moment in the experimentally visualized magnetic-domain pattern. The magnetic pattern in panel (b) is color coded as in Figure 2.

of the nanomembranes, various magnetic-domain patterns, such as magnetic spirals of various angles and azimuthally magnetized architectures, were created. We have found that the domain patterns characteristic of rolled-up architectures have a strong impact on their magnetic response and transport properties.

Azimuthally magnetized rolled-up nanomembranes are very attractive for application to magnetoimpedance-based field sensors, due to their enhanced and isotropic sensitivity compared with planar architectures. The fabrication of rolled-up single-layer magnetic architectures is of fundamental significance and its implications will extend far beyond the scope of the present work. One example is the prediction that in tubular structures unconventional magnetization dynamics may occur such as chirality-dependent domain-wall motion[24] enabling a Cherenkov-like effect for magnons in tubular architectures.[25] Experimental verification of these theoretical predictions not only requires substantial downscaling of rolled-up nanomembrane diameters, which may be achieved with epitaxially strained bilayers;[46] the development of suited characterization techniques, such as magnetic X-ray tomography, will become essential.

Acknowledgements

This work was supported in part by the Basic Science Research Program through a National Research Foundation of Korea funded by the Ministry of Science, ICT & Future Planning (Grant No. 2013003460) and via the German Science Foundation (DFG) grant MA 5144/2–1, DFG Research Unit 1713 and European Research Council under the European Union's Seventh Framework Programme (FP7/2007–2013)/ERC grant agreement no. 306277. The operation of the soft X-ray microscope was supported by the Director, Office of Science, Office of Basic Energy Sciences, Materials Sciences, and Engineering Division, of the U.S. Department of Energy under Contract No. DE-AC02–05-CH11231.

Received: July 1, 2013
Published online: October 18, 2013

[1] J. A. Rogers, T. Someya, Y. Huang, *Science* **2010**, *327*, 1603.
[2] O. G. Schmidt, K. Eberl, *Nature* **2001**, *410*, 168.
[3] D. H. Kim, J. L. Xiao, J. Z. Song, Y. G. Huang, J. A. Rogers, *Adv. Mater.* **2010**, *22*, 2108.
[4] D. H. Kim, N. Lu, R. Ma, Y. S. Kim, R. H. Kim, S. Wang, J. Wu, S. M. Won, H. Tao, A. Islam, K. J. Yu, T. Kim, R. Chowdhury, M. Ying, L. Xu, M. Li, H. J. Chung, H. Keum, M. McCormick, P. Liu, Y. W. Zhang, F. G. Omenetto, Y. Huang, T. Coleman, J. A. Rogers, *Science* **2011**, *333*, 838.
[5] F. Cavallo, M. G. Lagally, *Soft Matter* **2010**, *6*, 439.
[6] Y. F. Chen, Y. F. Mei, R. Kaltofen, J. I. Mönch, J. Schumann, J. Freudenberger, H. J. Klauß, O. G. Schmidt, *Adv. Mater.* **2008**, *20*, 3224.
[7] M. Melzer, D. Makarov, A. Calvimontes, D. Karnaushenko, S. Baunack, R. Kaltofen, Y. F. Mei, O. G. Schmidt, *Nano Lett.* **2011**, *11*, 2522.
[8] M. Melzer, D. Karnaushenko, D. Makarov, L. Baraban, A. Calvimontes, J. I. Mönch, R. Kaltofen, Y. Mei, O. G. Schmidt, *RSC Adv.* **2011**, *2*, 2284.
[9] M. Melzer, G. Lin, D. Makarov, O. G. Schmidt, *Adv. Mater.* **2012**, *24*, 6468.
[10] D. Karnaushenko, D. Makarov, C. Yan, R. Streubel, O. G. Schmidt, *Adv. Mater.* **2012**, *24*, 4518.
[11] Y. F. Mei, G. Huang, A. A. Solovev, E. Bermúdez-Ureña, I. Mönch, F. Die, T. Reindl, R. K. Y. Fu, P. K. Chu, O. G. Schmidt, *Adv. Mater.* **2008**, *20*, 4085.
[12] E. Bermúdez-Ureña, Y. F. Mei, E. Coric, D. Makarov, M. Albrecht, O. G. Schmidt, *J. Phys. D: Appl. Phys.* **2009**, *42*, 055001.
[13] F. Balhorn, S. Mansfeld, A. Krohn, J. Topp, W. Hansen, D. Heitmann, S. Mendach, *Phys. Rev. Lett.* **2010**, *104*, 037205.
[14] E. J. Smith, D. Makarov, O. G. Schmidt, *Soft Matter* **2011**, *7*, 11309.
[15] I. Mönch, D. Makarov, R. Koseva, L. Baraban, D. Karnaushenko, C. Kaiser, K.-F. Arndt, O. G. Schmidt, *ACS Nano* **2011**, *5*, 7436.
[16] C. Müller, C. C. Bof Bufon, M. E. Navarro-Fuentes, D. Makarov, D. H. Mosca, O. G. Schmidt, *Appl. Phys. Lett.* **2012**, *100*, 022409.
[17] F. Balhorn, S. Jeni, W. Hansen, D. Heitmann, S. Mendach, *Appl. Phys. Lett.* **2012**, *100*, 222402.
[18] A. A. Solovev, S. Sanchez, M. Pumera, Y. F. Mei, O. G. Schmidt, *Adv. Funct. Mater.* **2010**, *20*, 2430.
[19] E. J. Smith, D. Makarov, S. Sanchez, M. V. Fomin, O. G. Schmidt, *Phys. Rev. Lett.* **2011**, *107*, 097204.
[20] C. Deneke, J. Schumann, R. Engelhard, J. Thomas, C. Müller, M. S. Khatri, A. Malachias, M. Weisser, T. H. Metzger, O. G. Schmidt, *Nanotechnology* **2009**, *20*, 045703.
[21] C. Müller, M. S. Khatri, C. Deneke, S. Fähler, Y. F. Mei, E. Bermúdez-Ureña, O. G. Schmidt, *Appl. Phys. Lett.* **2009**, *94*, 102510.
[22] M. Yan, A. Kákay, S. Gliga, R. Hertel, *Phys. Rev. Lett.* **2010**, *104*, 057201.
[23] S. S. P. Parkin, M. Hayashi, L. Thomas, *Science* **2008**, *320*, 190.
[24] J. A. Otalora, J. A. Lopez-Lopez, P. Vargas, P. Landeros, *Appl. Phys. Lett.* **2012**, *100*, 072407.
[25] M. Yan, C. Andreas, A. Kákay, F. Garcia-Sanchez, R. Hertel, *Appl. Phys. Lett.* **2012**, *100*, 252401.
[26] D. Rüffer, R. Huber, P. Berberich, S. Albert, E. Russo-Averchi, M. Heiss, J. Arbiol, A. Fontcuberta i Morral, D. Grundler, *Nanoscale* **2012**, *4*, 4989.
[27] D. P. Weber, D. Rüffer, A. Buchter, F. Xue, E. Russo-Averchi, R. Huber, P. Berberich, J. Arbiol, A. Fontcuberta i Morral, D. Grundler, M. Poggio, *Nano Lett.* **2012**, *12*, 6139.
[28] B. Dieny, V. S. Speriosu, S. S. P. Parkin, B. A. Gurney, D. R. Wilhoit, D. Mauri, *Phys. Rev. B* **1991**, *43*, 1297.
[29] M. A. Ruderman, C. Kittel, *Phys. Rev.* **1954**, *96*, 99.
[30] S. S. P. Parkin, N. More, K. P. Roche, *Phys. Rev. Lett.* **1990**, *64*, 2302.
[31] N. Biziere, C. Gatel, R. Lassalle-Balier, M. C. Clochard, J. E. Wegrowe, E. Snoeck, *Nano Lett.* **2013**, *13*, 2053.
[32] R. Streubel, D. J. Thurmer, D. Makarov, F. Kronast, T. Kosub, V. Kravchuk, D. D. Sheka, Y. Gaididei, R. Schäfer, O. G. Schmidt, *Nano Lett.* **2012**, *12*, 3961.
[33] T. C. Penn, F. G. West, *J. Appl. Phys.* **1967**, *38*, 2060.
[34] L. W. McKeehan, P. P. Cio, *Phys. Rev.* **1926**, *28*, 146.
[35] X. Li, G. Ding, T. Ando, M. Shikida, K. Sato, *Microsyst. Technol.* **2008**, *14*, 131.
[36] A. Hubert, R. Schäfer, *Magnetic Domains – the Analysis of Magnetic Microstructures*, Springer-Verlag, Berlin Heidelberg, Germany **1998**.
[37] T. Schrefl, J. Fidler, *J. Magn. Magn. Mater.* **1992**, *111*, 105.
[38] K. Y. Guslienko, V. Novosad, Y. Otani, H. Shima, K. Fukamichi, *Phys. Rev. B* **2001**, *65*, 024414.
[39] J. Lee, D. Suess, T. Schrefl, K. H. Oh, J. Fidler, *J. Magn. Magn. Mater.* **2007**, *310*, 2445.

[40] P. Landeros, O. J. Suarez, A. Cuchillo, P. Vargas, *Phys. Rev. B* **2009**, *79*, 024404.
[41] A. P. Chen, K. Y. Guslienko, J. Gonzalez, *J. Appl. Phys.* **2010**, *108*, 083920.
[42] R. Skomski, J. Coey, *Permanent Magnetism*, Institute of Physics Publishing, Bristol, UK **1999**.
[43] P. Fischer, D.-H. Kim, W. Chao, J. A. Liddle, E. H. Anderson, D. T. Attwood, *Mater. Today* **2006**, *9*, 26.
[44] P. Fischer, T. Eimüller, G. Schütz, G. Denbeaux, A. Pearson, L. Johnson, D. Attwood, S. Tsunashima, M. Kumazawa, N. Takagi, M. Köhler, G. Bayreuther, *Rev. Sci. Instrum.* **2001**, *72*, 2322.
[45] D.-H. Kim, P. Fischer, W. Chao, E. Anderson, M.-Y. Im, S.-C. Shin, S.-B. Choe, *J. Appl. Phys.* **2006**, *99*, 8H303.
[46] C. Deneke, C. Müller, N. Y. Jin-Phillipp, O. G. Schmidt, *Semicond. Sci. Technol.* **2002**, *17*, 1278.